Sound Velocities and Elastic Moduli of Phases I and V of Silicon at High Pressures

Bin Zhao, Feng Xu, Laurent Belliard, Haijun Huang, Bernard Perrin, Philippe Djemia, and Andreas Zerr**

Pressure dependences of longitudinal sound velocities, in the two phases Si-I and Si-V of silicon having, respectively, cubic-diamond and primitive-hexagonal structures, are measured using the technique of picosecond laser ultrasonics adapted to samples compressed in a diamond anvil cell (DAC). For the Si-I phase, stable at atmospheric pressure, the longitudinal sound velocity along the ⟨100⟩ direction is obtained in a single crystal up to 9 GPa. In the case of the Si-V phase, the average sound velocity for an isotropic polycrystalline sample $V_{L(avg)}$ is measured for the first time between 18 and 27 GPa. Above this pressure, preferred orientation of the hexagonal crystallites of Si-V, with their *c*-axes parallel to the compressional direction in the DAC and to the acoustic pulse propagation direction, is progressively developing thus precluding further $V_{L(avg)}$ measurement. The experimental single crystal elastic constants $C_{11}(P)$ and $C_{12}(P)$ of Si-I, and the shear modulus of polycrystalline Si-V deduced here are in a very good agreement with our first principles calculations and with the earlier results reported for Si-I.

Silicon has come into wide use in semiconductor field and become the basic material due to its chemical, physical, and technical properties at atmospheric pressure. Upon compression, silicon metalizes and undergoes a series of phase transitions, and thus is considered as an example elemental solid in pressure-induced phase transition studies. Crystal structures, phase stability, related lattice dynamic properties were the subjects of intense experimental and theoretical interest over the past decades.[1–3] X-ray diffraction studies indicated that the sequential structural transitions of silicon with increasing pressure are as follows: cubic-diamond (Si-I) → β-Sn (Si-II)[4] → *Imma* (Si-XI)[5] → primitive-hexagonal (Si-V)[6] → *Cmca* (Si-VI)[6] → hexagonal closed-packed (Si-VII)[6] → face-centered cubic (Si-X, up to 248 GPa).[7] Si-II, Si-XI, and Si-VI phases are stable in quite narrow pressure regions,[8] and exist as single phases in even narrower regions due to coexistence with the adjacent phases. In contrast, Si-I, Si-V, Si-VII, and Si-X exist as single phases in extended pressure ranges. It was demonstrated that Si-I remains stable at $P < 9$ GPa,[6] and, between 18 and 38 GPa, only Si-V was observed.[9] While most of experimental high pressure studies on silicon were focused on crystal structures of the phases, only few works dealt with pressure dependences of elastic moduli of Si-I,[10–12] and, to our knowledge, no measurement of the shear modulus G or single crystal elastic constants C_{ij} of Si-V was reported yet.

Knowledge of sound velocities of solids at high pressures allows a better understanding of their intrinsic elastic properties, especially of $G(P)$, which is very sensitive to subtle phase transitions,[13] defects or inhomogeneities,[14] and permits a contrast-rich 3D tomography of non-uniform bodies.[15] However, measurement of sound velocities at high pressures is challenging, even using standard ultrasonic techniques or more recent synchrotron-based scattering techniques.[16] In contrast to standard ultrasonic techniques applicable in a limited pressure range, inelastic X-ray scattering permits measurement of longitudinal sound velocity V_L for a sample compressed in a DAC to very high pressures. However, it requires use of synchrotron radiation, large set-ups, very long counting times, and is only suited for samples containing elements with Z between 30 and 50.[16] The related technique of nuclear resonant inelastic X-ray scattering requires samples containing Mössbauer isotopes and theoretical modeling in order to extract sound velocities from the recorded signals. Thus, none of the last two techniques is suitable for the acoustic measurements on silicon samples in a DAC. At pressures above ≈20 GPa, combination of DAC with picosecond laser ultrasonics (PLU) provides access to sound velocities of opaque solids such as silicon.[17,18] Recently, the PLU based on phonon imaging was demonstrated to permit extraction of a complete set of C_{ij} of Si-I compressed in a DAC.[12]

B. Zhao, Dr. F. Xu, Prof. H. Huang
School of Science
Wuhan University of Technology
430070 Wuhan, China
E-mail: xufeng@whut.edu.cn

Prof. L. Belliard, Dr. B. Perrin
Sorbonne Université
UPMC Université Paris 06
CNRS UMR 7588
Institut des NanoSciences de Paris (INSP)
75005 Paris, France

Prof. P. Djemia, Dr. A. Zerr
Laboratoire des Sciences des Procédés et des Matériaux (LSPM)
UPR-CNRS 3407
Université Paris Nord
93430 Villetaneuse, France
E-mail: zerr@univ-paris13.fr

DOI: 10.1002/pssr.201900173

However, this method is less accurate when loading conditions become non-hydrostatic and deformations of the sample surface seriously influence the interferometric detection of the phonon imaging. Moreover, the acoustic mapping analysis requires single crystals which are difficult to preserve at ultrahigh pressures and upon phase transitions.

The pump-probe technique called time-domain Brillouin scattering (TDBS)[19] could be potentially applied to measure $V_L(P)$ of semiconducting Si-I, below ≈9 GPa, due to a relatively long optical penetration depth of the laser radiation with the wavelength $\lambda = 800$ nm. However, no Brillouin oscillations with frequencies above ≈78 GHz, expected for Si at 1 atm. or higher pressures, were observed in our trial TDBS experiments. For this reason, the PLU based on the pulse-echo method was applied to measure V_L of both Si-I and Si-V. Ultrafast acoustic pulses were generated and their arrivals detected by a conventional PLU setup equipped with a stabilized Michelson interferometer.[20] Briefly, a mode-locked Ti:sapphire laser (MAI-TAI Spectra, $\lambda = 800$ nm) operating with a repetition rate of 80 MHz and a pulse width of <100 fs was split into a pump and a probe beams. The photon frequency of the pump beam was doubled to ensure an efficient generation of acoustic pulses in silicon.[21] The beams were then focused on opposite sides of a sample with ×50 microscope objectives to spots of ≈2 μm in diameter (**Figure 1**). The probe beam measured the transient

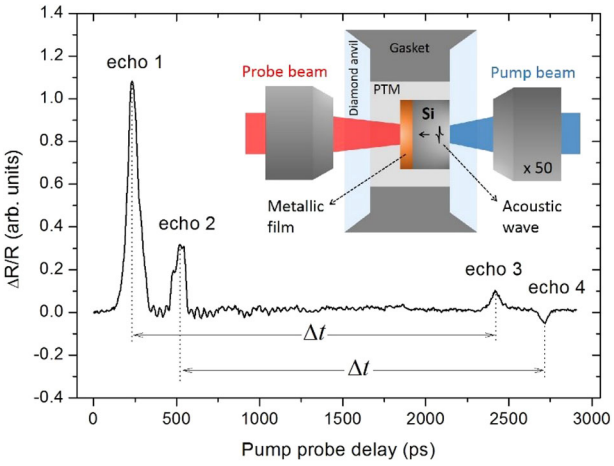

Figure 1. Relative change of reflectivity of the sample surface as a function of pump–probe delay recorded in the run 2 at $P = 6.3$ GPa. The acoustic pulse generated on the silicon side propagated in the sample and reflected from different interfaces. The echo 1 corresponds to the first arrival of the pulse on the opposite side. A part of it, reflected at the interface $FeSi_{0.2}$(1 μm thick film)/NaCl, returns as echo 2 after the roundtrip in the $FeSi_{0.2}$ film. The time intervals Δt between echoes 1 and 3 as well as echoes 2 and 4 correspond to the pulse roundtrip in silicon. The polarity of different echoes can be explained by acoustic reflectivity at the interfaces of the sample materials with different acoustic impedances:[20] the lowest one for NaCl, followed by Si and $FeSi_{0.2}$, and the highest for diamond. Brillouin oscillations,[19] visible after the arrival of the echo 1, result from interferences of the probe beam reflected from stationary surfaces and from the leaky acoustic pulse propagating in NaCl, used as the PTM. Inset: schematic representation of the sample inside a DAC. The pump beam is focused on the Si side while the probe beam on the $FeSi_{0.2}$ side.

reflectivity change of the sample surface, induced by arriving acoustic pulses, as a function of the time delay between the pump and probe beams. Three samples were studied in this work. These were single crystals of silicon having thicknesses of $h_0 = 9.74$ μm (subscript 0 indicates values at 1 atm.) which surfaces were oriented along (001) and covered with thin metallic films on one or both sides to enhance the photon-acoustic transduction efficiency. In present work, the $FeSi_{0.2}$ alloy and Ti were employed. Titanium is extensively used as a transducer in PLU because it exhibits strong photo-elastic coefficients in the near infrared range, when the photon energy is close to an interband transition.[22] However, delamination precludes deposition of thick Ti-films (>0.5 μm) needed for a reliable detection of acoustic pulse arrivals, especially at high pressures when the V_L increases and the film thickness decreases. In the first trial experiments (run 1) where both sample sides were covered with the metallic films, Ti(350 nm)/Si/$FeSi_{0.2}$(500 nm), we have found that $FeSi_{0.2}$ is well suited for acoustic pulse detection. Moreover, thick $FeSi_{0.2}$ films could be deposited on Si without delamination. Because acoustic pulses could be generated directly and efficiently on Si using the pump beam with $\lambda = 400$ nm,[21] samples covered with $FeSi_{0.2}$ films on one side, $FeSi_{0.2}$(1 μm)/Si, were used in the runs 2 and 3. The samples were compressed in a DAC with beveled diamond anvils having culets of 300 μm in diameter. A hole of ≈100 μm in diameter, drilled in a steel gasket pre-indented to the thickness of ≈40 μm, served as the sample volume. The samples were placed on one of the anvils and the remaining volume was filled with NaCl which served as a pressure transmitting medium (PTM) (Figure 1). Fluorescence of small ruby grains placed near the sample was used to measure pressure.[23]

All first-principles calculations in this work were based on the density functional theory (DFT) as implemented in the Vienna Ab-initio Simulation Package (VASP).[24,25] The total energy per atom was evaluated with 10^{-3} meV/atom convergence accuracy, for both cubic (space group $Fd\bar{3}mO1$) and hexagonal (space group $P63/mmc$) cells containing four and two atoms, respectively. The electron-ion interactions were described by the projector augmented wave method (PAW)[26] with a plane wave energy cutoff of 800 eV for cell optimizations, under the generalized gradient approximation (GGA) with a Perdew-Burke-Ernzerhof (PBE) exchange correlation functional.[27] The Monkhorst–Pack scheme[28] was used to construct k-meshes with 0.5 nm^{-1} spacing for self-consistent calculations.

An example of measured transient reflectivity used to extract V_L for one of our samples is shown in Figure 1. From such a record, the V_L value was determined using the relation: $V_L = 2h/\Delta t$, where Δt is duration of the acoustic pulse roundtrip in the silicon sample having thickness h. The latter was great enough to guarantee an excellent accuracy for the Δt determination (<5 ps) which corresponds to the V_L uncertainty below 0.2%. The sample thickness on compression was deduced from the measured here lateral area of the sample surface S and the earlier reported equation of state (EOS), $V(P)$.[2] At each pressure step, we recorded an optical image of the sample and used it to determine pressure dependence of the ratio $S(P)/S_0$. Dividing the known $V(P)/V_0$ for all silicon phases by our $S(P)/S_0$, we

obtained the relative thickness change $h(P)/h_0$. In the case of Si-I, the obtained dependence obeyed the earlier measured EOS: $h(P)/h_0 = [V(P)/V_0]^{1/3}$ which indicated that the loading conditions were close to hydrostatic and that the sample remained a single crystal till 9 GPa, close to the onset of the transition to Si-II. Above this transition, the correlation between $h(P)/h_0$ and $V(P)/V_0$ did not hold anymore thus suggesting plastic deformation of the sample due to growing non-hydrostaticity upon compression and low hardnesses of the high-pressure metallic phases of silicon. For this reason, thickness of the samples at $P > 10$ GPa was determined using the expression: $h(P) = h_0[V(P)/V_0][S_0/S(P)]$. We note that the $S(P)$ and, accordingly, $h(P)$ above 10 GPa was determined with the uncertainty of less than ≈2.5%, much larger than that of Δt.

Our experimental V_L values for all three runs are shown in **Figure 2**. Because Si-II and Si-XI coexist with the neighbor phases, and their volume ratios have not been well established in the literature, further analysis of the dependences $V_L(P)$ between 9 and 18 GPa was not meaningful. At pressures where only Si-I is present, up to 9 GPa, the measured $V_L(P)$ corresponds to that along ⟨100⟩. This is supported by the comparison with the value $V_{L\langle 100\rangle}(P)$ we calculated for the same direction in a single crystal of Si-I (Figure 2). Combining our $V_{L\langle 100\rangle}(P)$ and the EOS,[2] providing mass density $\rho(P)$ and bulk modulus $B(P)$, we derived pressure dependences of $C_{11}(P)$ and $C_{12}(P)$ using the well-known expressions: $C_{11} = \rho V^2_{L\langle 100\rangle}$ and $C_{12} = (3B - C_{11})/2$. In **Figure 3**, we compare our experimental and theoretical $C_{11}(P)$ and $C_{12}(P)$ with the earlier experimental and theoretical results.[10–12] An overall good agreement is found, even though our GGA values are ≈10% lower than those calculated within the local density approximation (LDA).

At pressures where only Si-V exists, between 18 and 38 GPa, our measured $V_L(P)$ increases slowly with compression up to ≈27 GPa. This dependence agrees with the $V_{L(avg)}(P)$ we calculated for a polycrystalline sample of Si-V with randomly oriented grains. The value of $V_{L(avg)}(P)$ is given by the expression: $V_{L(avg)} = \sqrt{(3B + 4G)/3\rho}$ where the isotropic moduli $B(P)$ and $G(P)$ were derived from our calculated $C_{ij}(P)$ and $\rho(P)$ using the Voigt–Reuss–Hill approximation. This observation indicated that up to ≈27 GPa the sample of Si-V was texture free. Applying the inverse equation $G = 3\left[\rho V^2_{L(avg)} - B\right]/4$ to our experimental data-points and the earlier measured $\rho(P)$ and $B(P)$, the experimental dependence $G(P)$ for a polycrystalline texture-free sample of Si-V was derived to 27 GPa (Figure 3).

It can be recognized in Figure 2 that above ≈27 GPa our experimental $V_L(P)$ increases much faster with pressure than below and strongly deviates from our theoretical $V_{L(avg)}(P)$. This suggests a significant texturing of the sample of Si-V upon compression above 27 GPa. Because the measured $V_L(P)$ approaches the maximal possible value in a hexagonal single crystal of Si-V (known to be along the *c*-axis, $V_{L\langle 0001\rangle}$), we may conclude that the developing texture was characterized by a growing number of grains which *c*-axes oriented along the propagation direction of the sound pulses, perpendicular to the anvil culets. This observation agrees with an earlier XRD work where strong changes in the intensity of the (001) and (100) peaks of Si-V were recognized at similar pressures.[7] We also show in Figure 2 $V_L(P)$ derived for the mixed phase region using our $S(P)/S_0$, an earlier EOS and the same equation

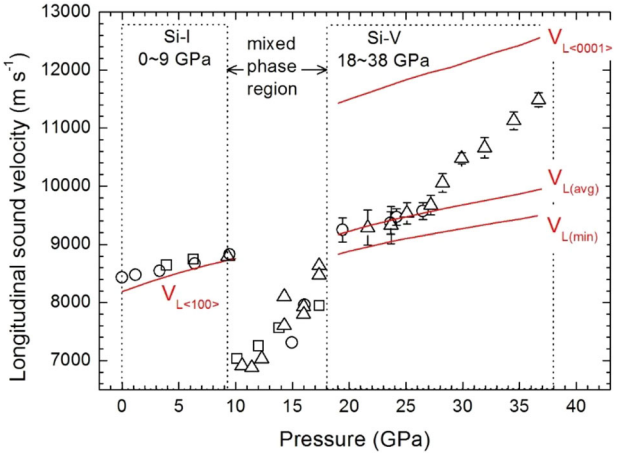

Figure 2. Longitudinal sound velocities of silicon as a function of pressure. The left and right framed ranges bracket pressures where only Si-I (0-9 GPa) and Si-V (18-38 GPa) exist. In the mixed phase region, the Si-I/Si-II, Si-II/Si-XI and Si-XI/Si-V may coexist (see text). The experimental data for the runs 1, 2, and 3 are shown by open circles, squares, and triangles, respectively. For the pure Si-I region, the experimental uncertainties in V_L are smaller than the symbols. Results of our first-principles calculations are presented by solid red lines: $V_{L\langle 100\rangle}$ is the sound velocity along ⟨100⟩ in Si-I, $V_{L(min)}$, and $V_{L\langle 0001\rangle}$ are the minimal and maximal values in a hexagonal single crystal of Si-V where $V_{L\langle 0001\rangle}$ corresponds to the velocity along the *c*-axis, $V_{L(avg)}$ is that derived for polycrystalline Si-V using our theoretical $C_{ij}(P)$, $\rho(P)$ and the Voigt–Reuss–Hill approximation.

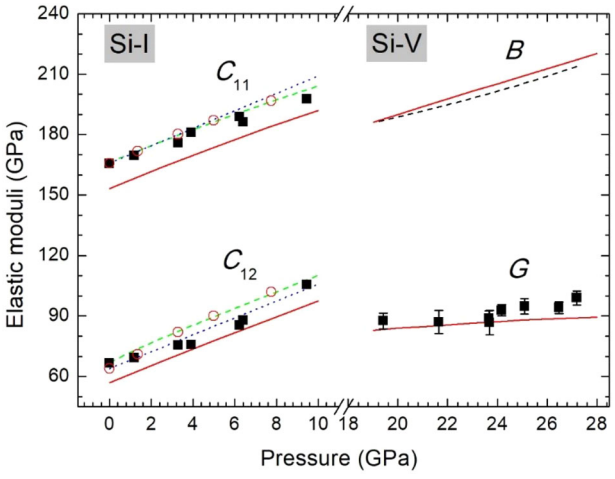

Figure 3. Pressure dependences of elastic moduli of the Si-I and Si-V phases. C_{11} and C_{12} indicate the corresponding single crystal elastic constants of Si-I. Our measured values (solid black squares) are compared with the earlier ones obtained by the phonon imaging method (open red circles)[12] and by a traditional ultrasonic technique (dotted blue lines).[10] Our ab initio results within GGA (solid red lines) are compared with the earlier predictions within LDA (dashed green lines).[11] Above 18 GPa, the solid black squares represent $G(P)$ of polycrystalline Si-V measured here and the dashed black line $B(P)$[2] measured earlier. Our theoretical $B(P)$ and $G(P)$ are represented by solid red lines.

$h(P) = h_0[V(P)/V_0][S_0/S(P)]$. Here, we assumed that above ≈10 GPa the sample contained Si-II and the following Si-XI phases only. This explains the sudden step-like decrease in $V_L(P)$ which should not appear in the case of an extended two phase region. These data were not further treated due to the absence of such information and are presented here only for completeness.

In conclusion, we investigated experimentally and theoretically pressure dependences of the longitudinal sound velocities and elastic moduli of Si-I and Si-V. Under compression, the starting single crystals of Si-I underwent phase transitions and polycrystalline phases with small randomly orientated grains appeared. After the three phase transitions, the samples of Si-V could be regarded as elastically isotropic. For the Si-I phase, the measured $V_L(P)$ corresponds therefore to that along the ⟨100⟩ direction, $V_{L\langle 100\rangle}(P)$. For Si-V, the measured $V_L(P)$ corresponds to that of an isotropic polycrystalline body $V_{L(avg)}(P)$ but only below 27 GPa. The dependences $C_{11}(P)$ and $C_{12}(P)$ of Si-I, we derived from the experimental $V_{L\langle 100\rangle}(P)$ using the earlier measured EOS, are in a very good agreement with previously published data and with our calculations. More important, we measured for the first time $V_L(P)$ and $G(P)$ for polycrystalline Si-V between 18 and 27 GPa. Above 27 GPa, we observed texturing of the polycrystalline Si-V whose grains preferably oriented with their *c*-axes along the compressional direction in the DAC.

Acknowledgements

The authors acknowledge financial support from NSFC (projects No. 41504070 and No. 41874103) and CSC (File No.201606955092). We would like to thank L. Becerra for sample preparation; E. Peronne for experimental assistance; Y. Wu and X. Liu for fruitful discussion. We acknowledge access to the cluster MAGI of University Paris 13 and N. Greneche for this support.

Conflict of Interest

The authors declare no conflict of interest

Keywords

elastic moduli, high-pressure phases, silicon, sound velocities

Received: March 21, 2019
Revised: April 17, 2019
Published online: May 8, 2019

[1] A. Mujica, A. Rubio, A. Munoz, R. J. Needs, *Rev. Mod. Phys.* **2003**, *75*, 863.
[2] R. J. Needs, A. Mujica, *Phys. Rev. B* **1995**, *51*, 9652.
[3] Y. He, L. Zhong, F. Fan, C. Wang, T. Zhu, S. X. Mao, *Nat. Nanotechnol.* **2016**, *11*, 866.
[4] J. C. Jamieson, *Science* **1963**, *139*, 762.
[5] M. I. McMahon, R. J. Nelmes, *Phys. Rev. B* **1993**, *47*, 8337.
[6] H. Olijnyk, S. K. Sikka, W. B. Holzapfel, *Phys. Lett. A* **1984**, *103*, 137.
[7] S. J. Duclos, Y. K. Vohra, A. L. Ruoff, *Phys. Rev. B* **1990**, *41*, 12021.
[8] M. I. McMahon, R. J. Nelmes, N. G. Wright, D. R. Allan, *Phys. Rev. B* **1994**, *50*, 739.
[9] M. Hanfland, U. Schwarz, K. Syassen, K. Takemura, *Phys. Rev. Lett.* **1999**, *82*, 1197.
[10] H. J. McSkimin, P. Andereatch, *J. Appl. Phys.* **1964**, *35*, 2161.
[11] B. B. Karki, G. J. Ackland, J. Crain, *J. Phys. Condens. Mat.* **1997**, *9*, 8579.
[12] F. Decremps, L. Belliard, M. Gauthier, B. Perrin, *Phys. Rev. B* **2010**, *82*, 104119.
[13] N. Cai, T. Chen, X. Qi, B. Li, *J. Appl. Phys.* **2018**, *124*, 185901.
[14] Y. Wang, D. H. Hurley, Z. Hua, G. Sha, S. Raetz, V. E. Gusev, M. Khafizov, *Scr. Mater.* **2019**, *166*, 34.
[15] P. Clouzet, Y. Masson, B. Romanowicz, *Geophys. J. Int.* **2018**, *213*, 1849.
[16] R. J. Angel, J. M. Jackson, H. J. Reichmann, S. Speziale, *Eur. J. Mineral.* **2009**, *21*, 525.
[17] F. Decremps, L. Belliard, B. Perrin, M. Gauthier, *Phys. Rev. Lett.* **2008**, *100*, 035502.
[18] F. Decremps, M. Gauthier, S. Ayrinhac, L. Bove, L. Belliard, B. Perrin, M. Morand, G. Le Marchand, F. Bergame, J. Philippe, *Ultrasonics* **2015**, *56*, 129.
[19] S. M. Nikitin, N. Chigarev, V. Tournat, A. Bulou, D. Gasteau, B. Castagnede, A. Zerr, V. E. Gusev, *Sci. Rep.* **2015**, *5*, 9352.
[20] F. Xu, L. Belliard, D. Fournier, E. Charron, J.-Y. Duquesne, S. Martin, C. Secouard, B. Perrin, *Thin Solid Films* **2013**, *548*, 366.
[21] K. Ishioka, A. Rustagi, U. Hofer, H. Petek, C. J. Stanton, *Phys. Rev. B* **2017**, *95*, 035205.
[22] A. Devos, A. Le Louarn, *Phys. Rev. B* **2003**, *68*, 045405.
[23] H. K. Mao, J. Xu, P. M. Bell, *J. Geophys. Res. Sol. Ea.* **1986**, *91*, 4673.
[24] G. Kresse, J. Hafner, *Phys. Rev. B* **1993**, *47*, 558.
[25] G. Kresse, J. Furthmüller, *Comput. Mater. Sci.* **1996**, *6*, 15.
[26] G. Kresse, D. Joubert, *Phys. Rev. B* **1999**, *59*, 1758.
[27] J. P. Perdew, K. Burke, M. Ernzerhof, *Phys. Rev. Lett.* **1996**, *77*, 3865.
[28] H. J. Monkhorst, J. D. Pack, *Phys. Rev. B* **1976**, *13*, 5188.

